CSIRO PUBLISHING

Australian Journal of Physics

Volume 51, 1998
© CSIRO 1998

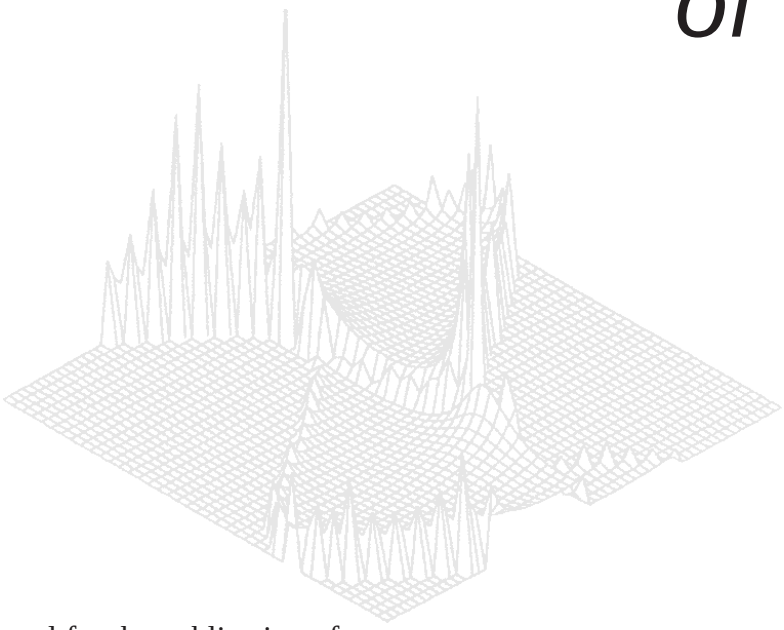

A journal for the publication of
original research in all branches of physics

www.publish.csiro.au/journals/ajp

All enquiries and manuscripts should be directed to
Australian Journal of Physics
CSIRO PUBLISHING
PO Box 1139 (150 Oxford St)
Collingwood Telephone: 61 3 9662 7626
Vic. 3066 Facsimile: 61 3 9662 7611
Australia Email: peter.robertson@publish.csiro.au

Published by **CSIRO** PUBLISHING
for CSIRO and the
Australian Academy of Science

Aust. J. Phys., 1998, **51**, 593–607

The Development of Electron Momentum Spectroscopy*

Ian E. McCarthy

Department of Physics, Flinders University of South Australia,
GPO Box 2100, Adelaide, SA 5001, Australia.

Abstract

Electron momentum spectroscopy measures relative differential cross sections as a function of recoil momentum for energy-resolved states of the ion in a kinematically-complete electron-impact ionisation experiment. The experiment is done in a kinematic range where correct cross sections are obtained by simple reaction approximations. It amounts to a measurement of orbital momentum densities and coefficients describing electron correlations in the ion for most ion states of a gas target. Certain ion states give information about ground-state correlations. For a solid target it amounts to a measurement of the energy–momentum density of occupied electron bands.

1. Introduction

The development of electron momentum spectroscopy (EMS), from the first experiment that resolved valence states (Weigold *et al.* 1973) to its present-day applications in condensed-matter physics and quantum chemistry, is synonymous with the name of Erich Weigold. Examples of the applications are given by Canney *et al.* (1997) and Adcock *et al.* (1997).

When Erich came to Flinders in 1970 he began to set up an experiment to observe the energy and momentum of two electrons in coincidence, arising from an ionising collision of an electron in an energy-resolved and collimated beam with an atom or molecule in a gas target. Before the first results were produced in 1973, he had been encouraged by the successful observation of coincidences for an atomic target at Kaiserslautern (Ehrhardt *et al.* 1969) and a series of experiments for solid targets at Frascati that culminated in the measurement of the momentum distribution of the 1s electron of solid carbon (Camilloni *et al.* 1972).

The (e, 2e) experiment observes the momentum $\mathbf{p}_0, \mathbf{p}_A$ and $\mathbf{p}_B$ and kinetic energy E_0, E_A and E_B of each of the three electrons 0 (incident), A and B (outgoing) involved in an ionising event that is part of a large ensemble of such events. The recoil momentum $\mathbf{p}$ and separation (or binding) energy ϵ are obtained by subtracting the corresponding final-state values from the initial-state values:

$$\mathbf{p} = \mathbf{p}_0 - \mathbf{p}_A - \mathbf{p}_B \,, \tag{1}$$

* Dedicated to Professor Erich Weigold on the occasion of his sixtieth birthday.

© CSIRO Australia 1998 10.1071/PH97081 0004-9506/98/040593$05.00

$$\epsilon = E_0 - E_A - E_B \,. \tag{2}$$

For gas targets the energy ϵ, within limits imposed by experimental resolution of the order of 1 eV, defines discrete groups of events, each corresponding to the eigenvalue ϵ_i of an ion state i. In the usual case of random target orientation there is a distribution of absolute recoil momentum p, the momentum profile $F_i(p)$, that is characteristic of the state i. This is the spherical average of profiles $F_i(\mathbf{p})$ for oriented target systems.

The naive interpretation of the experiment, which is modified but not invalidated under some experimental conditions, forms the intuitive basis for EMS. If we assume that momentum is transferred to the external electrons only by the elementary collision, and not by interactions with other parts of the target system, then the recoil momentum $\mathbf{p}$ is equal and opposite to the momentum $\mathbf{q}$ of the struck electron:

$$\mathbf{q} = -\mathbf{p} \,. \tag{3}$$

This is essentially the plane-wave impulse approximation (PWIA), so called because the motion of an electron with no change of momentum is described by a plane wave. As the energies of the external electrons are increased this approximation increases in validity. The beauty of the experiment is that, because bound-electron energies and momenta are determined by subtraction, the only limit on the external energies is provided by experimental feasibility.

The first question to be answered by early experiments was: do practical experiments approach the PWIA limit sufficiently closely for the naive interpretation to have practical validity? The second question depends on the structure of bound-electron systems. We know already that the independent-particle model has some validity. Here the momentum profile of an electron occupying an orbital α is the absolute square of the momentum-space wave function

$$F_\alpha(\mathbf{q}) = |\phi_\alpha(\mathbf{q})|^2 \,. \tag{4}$$

The question is: how is the observed profile $F_i(p)$ related to an independent-particle profile $F_\alpha(\mathbf{q})$, assuming the PWIA (3)?

The first EMS experiment had a target of argon atoms. It observed the momentum profiles for several resolved states of the ion. In nuclear physics (p, 2p) experiments on light nuclei, see for example Garron *et al.* (1962), had observed vestiges of the proton momentum distributions for resolved final states expected on the basis of the independent-particle model. We had hoped that the (e, 2e) experiments would observe something analogous and were totally unprepared for the brilliant clarity of the first results and of follow-up experiments performed shortly after.

2. Ion-state Spectroscopy illustrated by the Argon Atom

The distribution of final-state energies for a recoil momentum $p = 0{\cdot}47$ a.u. in the first experiment on argon is shown in Fig. 1. The total energy

$$E = E_A + E_B \tag{5}$$

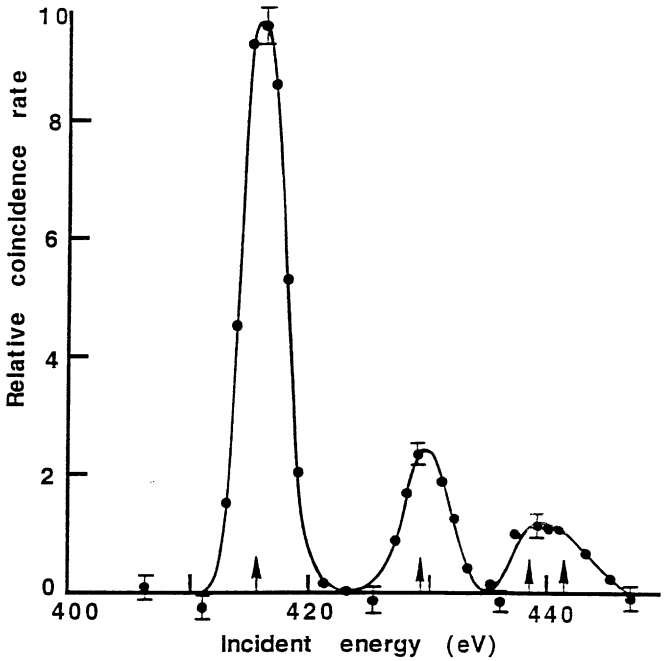

Fig. 1. Relative differential cross section at $p = 0{\cdot}47$ a.u. for the ionisation of argon (Weigold *et al*. 1973). The arrows indicate known energy levels of the argon ion.

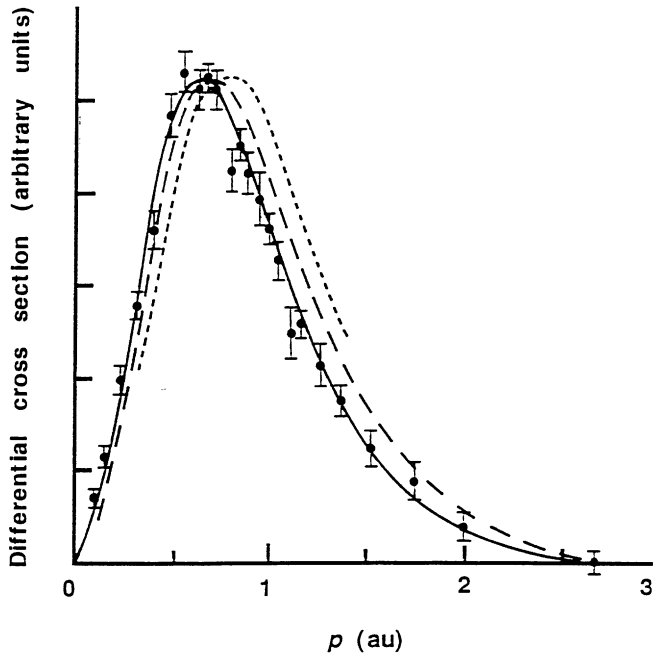

Fig. 2. The 1200 eV momentum density for the $15{\cdot}8$ eV state of the argon ion (McCarthy and Weigold 1988). PWIA curves are calculated with 3p orbitals. Full curve: Hartree–Fock, long-dashed curve: Hartree–Fock–Slater, and short-dashed curve: minimal variational basis.

was 400 eV. The separation energy ϵ was scanned by varying E_0. The absolute momentum p was scanned in noncoplanar symmetric kinematics. Here $E_A = E_B$, the polar angles θ_A and θ_B, measured from the direction of $\mathbf{p}_0$, are both 45°, and p is scanned from close to 0 to about 2 a.u. by varying the relative azimuthal angle ϕ.

The Hartree–Fock calculation, which is the independent-particle model with the minimum variational energy, predicts the 3p orbital at $\epsilon_{3p} = 15{\cdot}8$ eV, and the 3s orbital at $\epsilon_{3s} = 34{\cdot}8$ eV. The experiment observed three energy peaks, the third of which contained at least two ion states that had been resolved by photon spectroscopy. Clearly this structure is already more complicated than the independent-particle description.

Now the momentum dimension of the experiment plays its part. This was very clear in the first experiment, but is illustrated better by two of the follow-up experiments. The first, for 1200 eV in Fig. 2, shows that $F_{15\cdot8}(p)$ is described

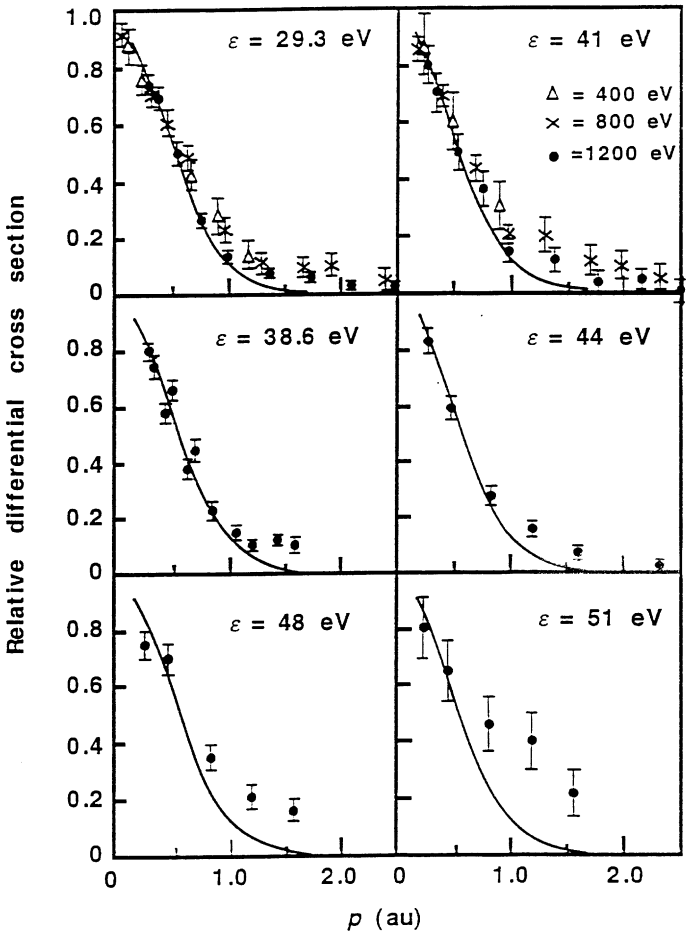

Fig. 3. Momentum density at the indicated energies for the ionisation of argon to states above the argon ground state (McCarthy and Weigold 1976). Full curves: PWIA for the Hartree–Fock 3s orbital.

within the 10 per cent experimental statistical error by the 3p Hartree–Fock orbital, but not by orbitals from the less-detailed but plausible Hartree–Fock–Slater and minimal-variational calculations. Not only is the independent-particle approximation confirmed for this case, but it is defined with great precision. The 15·8 eV ion state is described as a 3p hole in the independent-particle configuration of the target.

What about the higher ion states? Their momentum-profile shapes, in some cases for widely-differing total energies, are shown in Fig. 3. Up to about 1 a.u. their momentum profiles are all given by the 3s Hartree–Fock orbital, which gives an underestimate for higher momenta. It was certain that the momentum profiles reflected genuine structure information because they were independent of energy. What are they telling us? Clearly the independent-particle model is valid in the sense that it describes the momentum profiles. Since the momentum profile is a probability, it is clearly the probability that the ion state i is described by the model. There is a manifold of ion states, the 3s orbital manifold, all of which have a certain probability of being in a configuration described by the 3s-hole model, identified by the 3s momentum-profile shape, whose probabilities for the 3s hole must sum to 1. Since this must be true also for the 3p hole, the unique 3p-hole state defines unit probability so that we can check the whole interpretation by comparing relative magnitudes of momentum profiles.

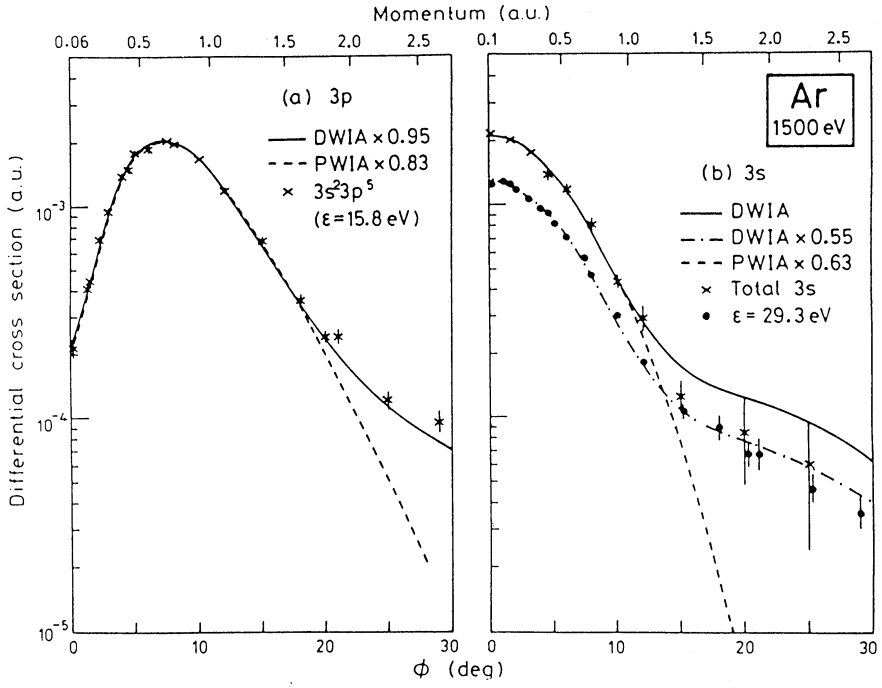

Fig. 4. The 1500 eV momentum density for (a) the 3p and (b) the 3s manifolds of argon (McCarthy *et al.* 1989). The experimental angular resolution has been folded into the calculated cross sections.

We can thus reconstruct an experimental orbital from the orbital manifold. What about the orbital energy? It is the centroid of the manifold energies weighted by their probabilities, the spectroscopic factors.

We summarise our understanding by considering an orbital manifold for the orbital α. Each state $i \in \alpha$ has the momentum profile $F_\alpha(q)$ characteristic of α. The weight of the state i in the manifold, given by the relative magnitude of its momentum profile, is the spectroscopic factor S_i^α:

$$F_i(q) = S_i^\alpha F_\alpha(q)\,. \tag{6}$$

The spectroscopic factors are put on an absolute scale, which is the same for all orbital manifolds, by the sum rule

$$\sum_{i\in\alpha} S_i^\alpha = 1\,. \tag{7}$$

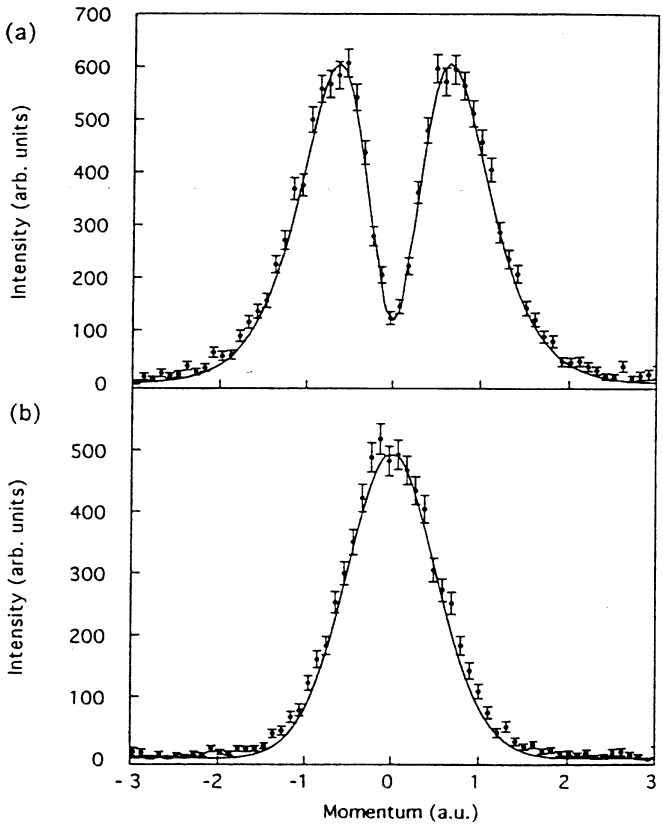

Fig. 5. The 20 keV EMS momentum densities for the (a) 15·8 eV and (b) 27·2 eV ion states of argon (Storer *et al.* 1994). Curves show the PWIA. Parts (a) and (b) are relatively normalised with previously-measured spectroscopic factors.

The orbital energy is the centroid of the manifold energies:

$$\epsilon_\alpha = \sum_{i\in\alpha} S_i^\alpha \epsilon_i \,. \tag{8}$$

The whole understanding of the argon valence states summarises the analysis of ion-state spectroscopy by EMS. It is illustrated in Fig. 4. Here the 1500 eV experimental data are compared with the distorted-wave impulse approximation (DWIA), which modifies the high-energy plane-wave analysis by including the elastic scattering of the external electrons in the calculation. Hartree–Fock orbitals are used. The absolute scale is determined by fitting the 3p data to the DWIA. Both the 3s manifold and its most-intense state at 29·2 eV are perfectly described by the calculation in magnitude and shape of the momentum profile. The 29·2 eV spectroscopic factor is 0·55. This is obtained by using a spectroscopic factor $S^{3p}_{15\cdot 8} = 0\cdot 95$, determined after observing higher states of the 3p manifold in detailed experiments (McCarthy *et al.* 1989). We note that, as in Fig. 3, the PWIA underestimates the high-momentum magnitudes. This shortcoming of the PWIA at energies near 1 keV is corrected by the DWIA. The 3s orbital energy, determined from the 3s manifold, is $35\cdot 2 \pm 0\cdot 2$ eV. The validity of the PWIA at very high energies is shown by the 20 keV experiment for argon in Fig. 5. This experiment was used to check the new spectrometer that is now used at Flinders for solid films. The data are all fitted to the PWIA at one point using $S^{3s}_{29\cdot 2} = 0\cdot 55$.

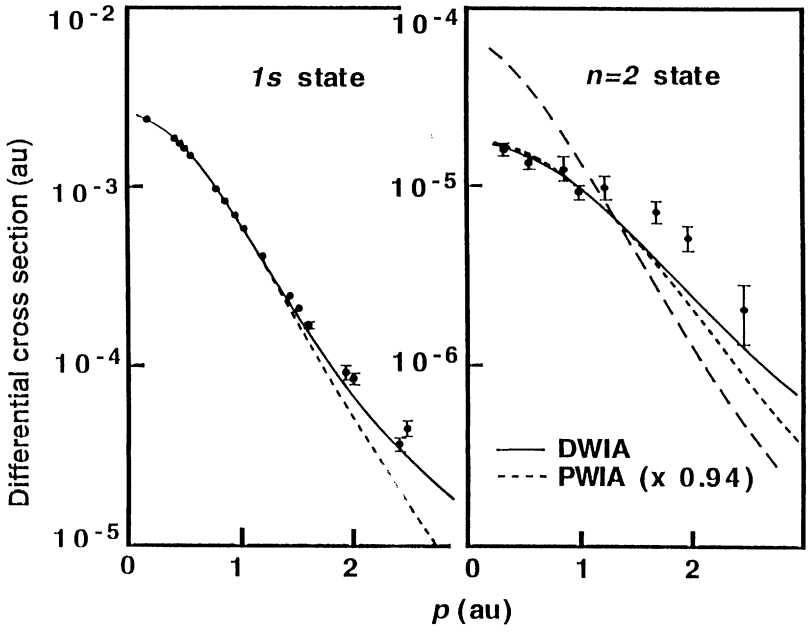

Fig. 6. The 1200 eV momentum densities for the $n = 1$ and summed $n = 2$ transitions in helium (Cook *et al.* 1984). DWIA and PWIA curves (McCarthy and Mitroy 1988) are indicated. The long-dashed curve is the DWIA for the Hartree–Fock ground state. Experimental data are normalised to the $n = 1$ curve.

3. Atoms

The first big advance in the understanding of electronic systems that can be achieved by EMS came very early in its history (McCarthy *et al.* 1974). Erich decided to look for the unresolved $n = 2$ ion states at $54{\cdot}4$ eV in the EMS of helium. Since the independent-particle model of the $^1S_0$ helium ground state has two 1s electrons, a finite probability of observing the 2p ion state would mean a finite probability of the ground state containing a configuration such as $2p^2$. The 2s situation is not quite so clearcut, since any s orbital is a linear combination of ns orbitals, depending on their definition. Thus EMS is sensitive to ground-state correlations. The $n = 2$, and later $n = 3$ (Cook *et al.* 1984), ion states were observed with momentum profiles that are well described by the DWIA with a correlated ground state obtained from a configuration-interaction calculation (McCarthy and Mitroy 1986). Here the target Hamiltonian is diagonalised in a basis of configurations formed by occupying ground-state Hartree–Fock orbitals with electrons in such a way that all configurations have the symmetry of the ground state. This is shown in Fig. 6.

In general ground-state correlations are observed by identifying ion states whose momentum profiles are not described by single orbitals. Such states have small intensities in the experiment and are likely in most cases to be hard to resolve from nearby more-intense states.

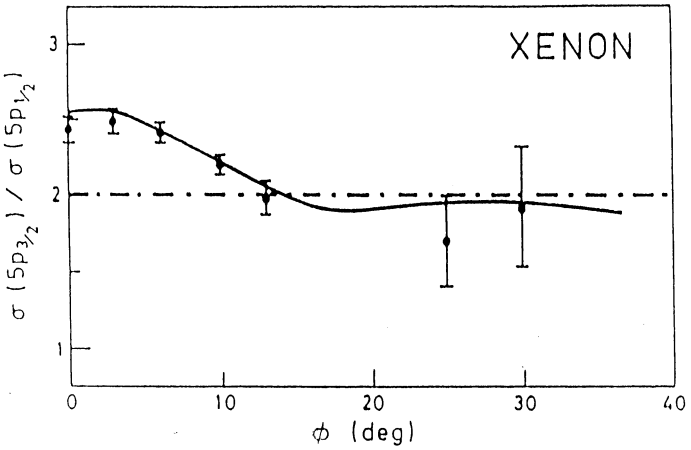

Fig. 7. Ratio of $5p_{3/2}$ to $5p_{1/2}$ differential cross sections for xenon at 1000 eV (Cook *et al.* 1986). Full curve: DWIA with Dirac–Fock orbitals, broken line: nonrelativistic branching ratio.

Experiments on atoms have illustrated further points. An important one is the validity of the relativistic Dirac–Fock calculation of the valence orbitals of xenon (Cook *et al.* 1986). At the time this calculation (Grant 1970) was intuitively appealing but not fully justified. For xenon it is possible to resolve the spin–orbit splitting so that momentum profiles can be obtained for $5p_{1/2}$ and $5p_{3/2}$ orbitals. They are so different that the ratio of their momentum profiles depends on momentum. This is obtained within experimental error by the Dirac–Fock calculation in the DWIA (Fig. 7).

The first experiment on an excited and oriented target was performed on sodium atoms, excited into the $m = 1$ magnetic substate of the $3^2P_{3/2}$ state by optical pumping with σ^+ circularly-polarised laser light (Zheng *et al.* 1990).

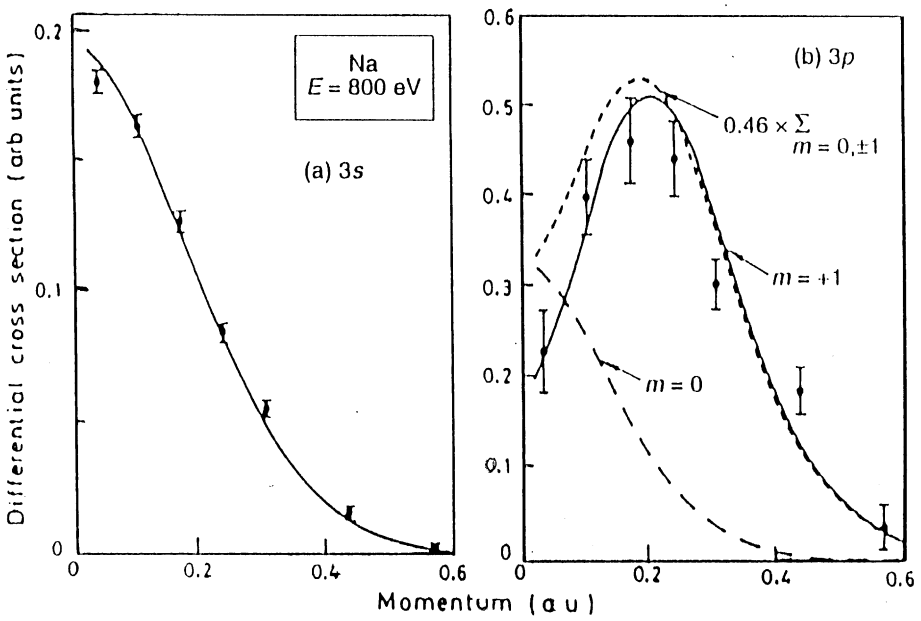

Fig. 8. The 800 eV momentum profiles for the laser-assisted ionisation of sodium (Zheng *et al.* 1990). Hartree–Fock curves for the indicated states are calculated in the PWIA.

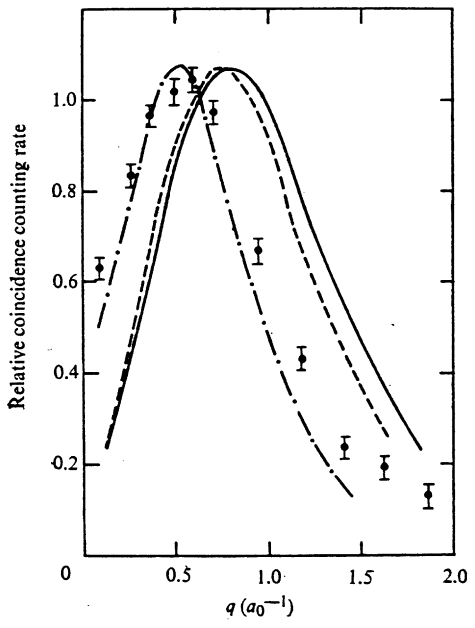

Fig. 9. Momentum profile at 400 eV for the $1t_2$ orbital of methane (Hood *et al.* 1973). PWIA curves are as follows. Full curve: Pitzer (1967), dashed curve: Palke and Lipscomb (1966), and dot–dash curve: carbon 2p Hartree–Fock (Froese-Fischer 1972).

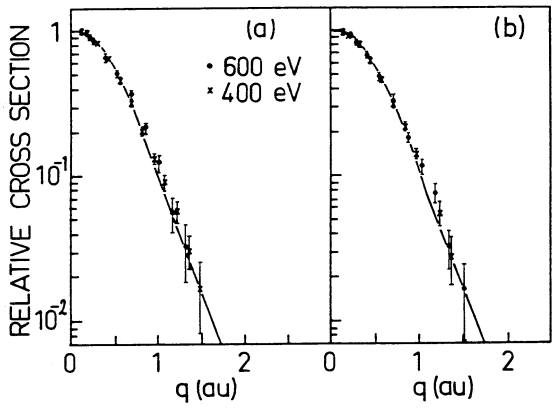

Fig. 10. Momentum densities for (a) H_2 and (b) D_2 at 600 eV (filled circles) and 400 eV (crosses) (Dey *et al.* 1975). The PWIA curve is a vibrational average computed with the configuration-interaction ground state of McLean *et al.* (1960).

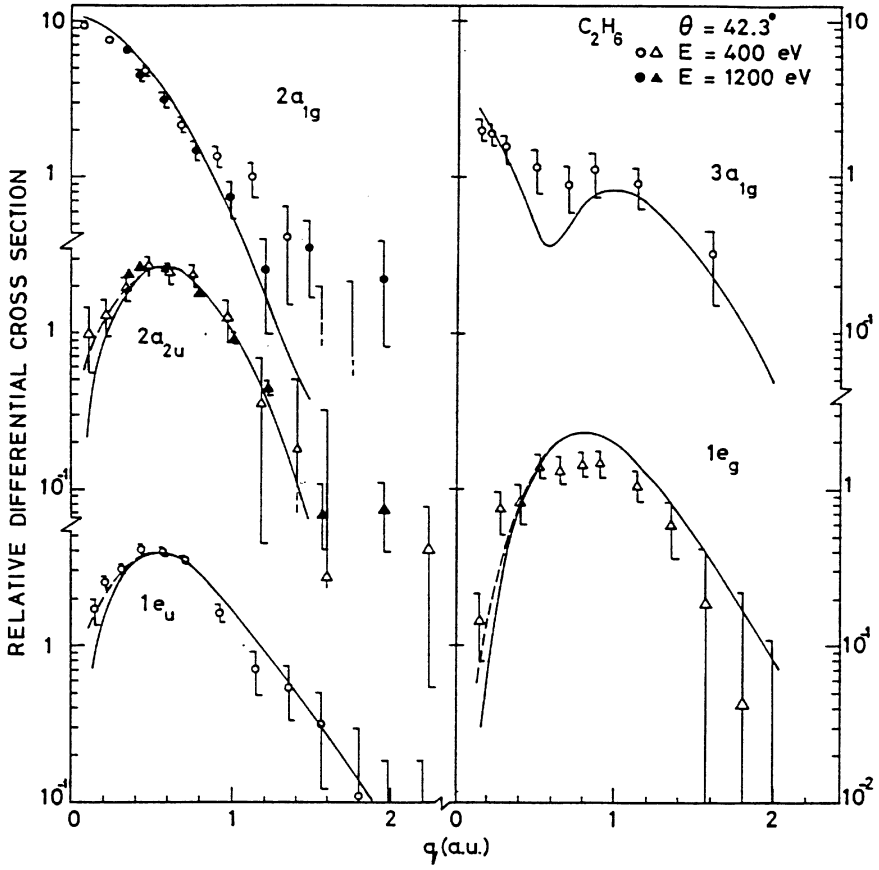

Fig. 11. Momentum densities for ethane (Dey *et al.* 1976) at 400 eV (open symbols) and 1200 eV (filled symbols), normalised to the PWIA for the $1e_u$ case at 0·6 a.u. The solid curves indicate the PWIA. The dashed curves have experimental angular resolution folded into the PWIA.

Fig. 8 shows the agreement of the 800 eV experiment for the ground and excited states with the PWIA using Hartree–Fock orbitals.

4. Molecules

The first molecule to be observed by EMS was methane (Hood *et al.* 1973). As in the case of the argon atom the sensitivity of the momentum profile to the description of the corresponding orbital was demonstrated very dramatically by the p-like orbital (Fig. 9), in this case $1t_2$. Two very simple molecular orbitals (Pitzer 1967; Palke and Lipscombe 1966) were completely inadequate. This orbital is dominated by the carbon 2p component and it is not surprising that the Hartree–Fock carbon 2p orbital of Froese-Fischer (1972) obtained a much better peak momentum.

The first results for the hydrogen molecule (Weigold *et al.* 1973) were significant for the fact that the momentum-profile shape was the same for $E = 400$ eV and 1000 eV, thus providing early confirmation of the validity of the structure information contained in the data. A later experiment on H_2 and D_2 (Dey *et al.* 1975) demonstrated a very important fact that underlies the whole analysis of molecules by EMS. What is observed is the target-ion electronic structure at the equilibrium positions of the nuclei. Differential cross sections are spherically averaged to account for the random orientations of the target molecules. Vibrational and rotational states play no part. H_2 and D_2 have nuclear masses that differ by a factor of 2 and for this reason their vibrational states are very different. Nevertheless the momentum-profile shapes for the two cases agree over two orders of magnitude. They are well described by a PWIA calculation using sophisticated target and ion electronic wave functions. Inclusion of vibrational states made no difference. This is shown in Fig. 10.

The analysis of ethane (Dey *et al.* 1976) is shown in Fig. 11. It is typical of many small molecules. First, the validity of the structure information is confirmed by the agreement of momentum-profile shapes and relative magnitudes for the five valence orbitals at $E = 400$ eV and 1200 eV. Small-basis molecular orbitals (Snyder and Basch 1972) give excellent profile shapes and confirm the spectroscopic sum rule (7).

Water forms a very interesting contrast for the p-like valence orbitals. The experiment of Dixon *et al.* (1977) showed that the molecular orbitals of Snyder and Basch underestimate the low-momentum density by a large factor. A calculation using many-body perturbation theory corrected all but the $1b_1$ (outermost) case, suggesting that the discrepancy was due to the neglect of ground-state correlations relative to Hartree–Fock orbitals. This is illustrated in Fig. 12. The interpretation was confirmed in a very detailed analysis by Bawagan *et al.* (1987), which showed that converged Hartree–Fock orbitals were still inadequate but a converged many-body calculation agreed with the momentum profiles. Incidentally this analysis gives strong confirmation of the validity of the PWIA for molecules. The failure of simple molecular orbitals for low momenta has been observed for other second-row hydrides, for example ammonia (Hood *et al.* 1976). The question of whether a self-consistent target orbital calculation is able to account for sufficient many-body effects was answered for water by Duffy *et al.* (1994), who showed that the shape discrepancy for water is corrected by target orbitals calculated by density-functional theory, which includes a correlation term in the effective one-electron potential.

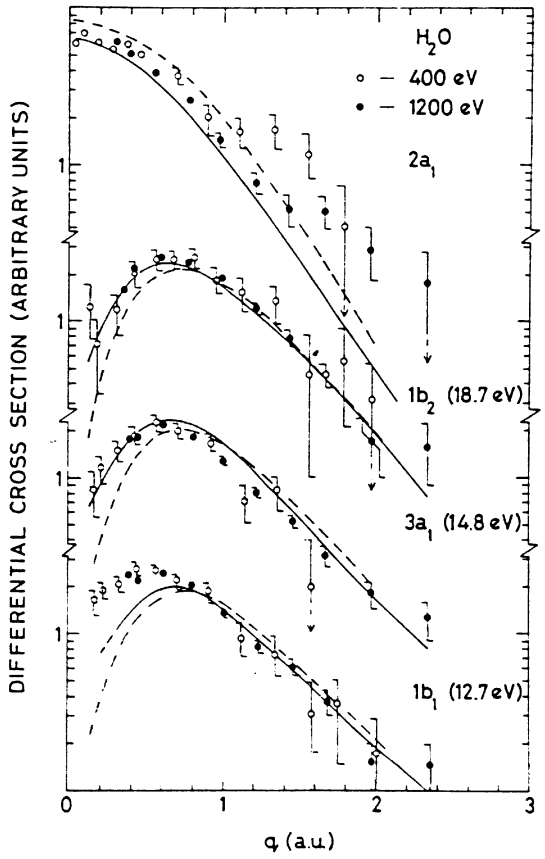

Fig. 12. Momentum profiles for the four valence states of water (Dixon *et al.* 1977). DWIA curves are calculated for the following structure approximations. Full curve: many-body perturbation theory, and dashed curve: Snyder and Basch (1972).

5. Solids

In the case of solids, instead of the momentum density for resolved ion states, one expects to observe the energy–momentum density for electron bands that exhibit dispersion. The experimental difficulty for solid targets is much greater than for gases. In order to observe momentum from zero to higher values it is necessary to observe electrons transmitted through the target sample. Sample preparation is therefore not trivial. The thickness must be of the order of the mean free path of electrons, which is about 10 nm for kinetic energies of order 10 keV. Under such conditions count rates are low and radical improvements to the detection system are necessary to achieve adequate energy resolution for adequate count rate. It is also necessary to characterise the sample and maintain it free from contamination for the duration of the experiment. The special research centre for the electronic structure of materials that was set up at Flinders in 1988 made it possible to construct the necessary equipment.

For about the first ten years of EMS, detectors were set up to observe a single energy and a single momentum for each run in an energy–momentum scan. In a one-dimensional multiparameter detection system, electrons are first passed through an energy-dispersing element before impinging on a position-sensitive detector in order to perform a simultaneous measurement over a broad range of energies. This considerably improves the count rate for a given energy resolution and was used for the earliest experiments on solids at Flinders, which were not, however, the first in the field.

Valence-band energy–momentum structures were first resolved by Ritter *et al.* (1984) for evaporated amorphous carbon with 6 eV resolution. These results were confirmed by Hayes *et al.* (1990) and Lower *et al.* (1991) with improved energy resolution. Clear evidence was obtained that EMS could provide new information on the electronic structure of solids. All these experiments were severely limited by count rates of order one per minute.

Detailed EMS of thin solid films became feasible in 1993 when the Flinders spectrometer was commissioned (Storer *et al.* 1994). Two-dimensional multiparameter detectors, for a range of separation energy from 0 to 50 eV and momentum from −3 a.u. to 3 a.u. in a direction normal to the mean detection plane, made possible count rates of several hundred per minute with energy resolution about 1 eV, sufficient to resolve bands, and momentum resolution about 0·15 a.u. A complete experiment for a given target took a few days. The 20 keV incident electrons had a mean free path of about 10 nm. The 2 nm mean free path of the slower (1·2 keV) outgoing electrons restricted the observed region to within 2 nm of the exit surface.

The main points of valence EMS on an amorphous solid are illustrated by Fig. 13 for evaporated aluminium (Canney *et al.* 1997), which is essentially a

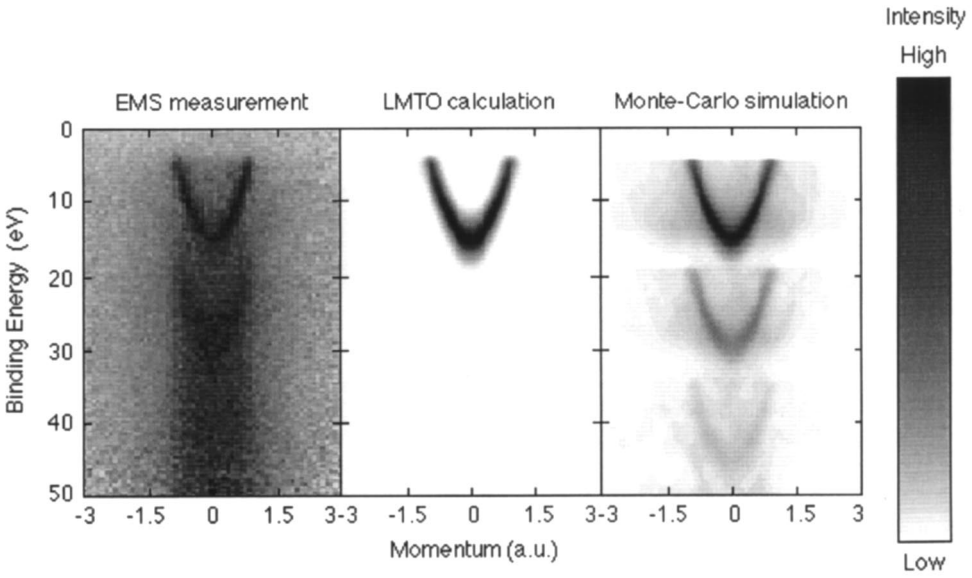

Fig. 13. The energy–momentum density of polycrystalline aluminium (Canney *et al.* 1997). Details are given in the text.

free-electron metal. The dispersion curve of separation energy ϵ *vs* momentum q is expected to be a free-electron parabola, given in atomic units by

$$\epsilon = \epsilon_0 - q^2/2m^* \,, \tag{9}$$

where the shape of the parabola is given by the effective mass m^*, which is equal to 1 for a free electron. The occupation density of the valence-band parabola is expected to be a Fermi distribution, uniform up to a cutoff at the Fermi level. A grey-scale representation of the experimental data is shown in the first panel of Fig. 13. The parabola has the expected density feature. It is broadened by energy resolution and the effect of the finite lifetime of the hole left behind by removing the electron. Momentum broadening is due to the effects of phonon excitation as well as resolution. An independent-particle-model calculation that incorporates appropriate broadening is shown in the second panel.

The experiment shows two features in addition to the valence-band parabola. They are essentially broadened versions of the valence band at separation energies about 15 eV and 30 eV greater. They are attributed to the excitation of one or two plasmons, which are vibrational modes of the plasma set up by the electron gas and the background ions. A detailed understanding of the experiment is illustrated in the third panel of Fig. 13, which shows the results of a Monte-Carlo calculation for electron trajectories by Vos and Bottema (1996), where branching probabilities are given by theoretical estimates of the cross sections for electron–atom collisions, in which the recoil excites a phonon, and for bulk-plasmon excitation.

This section has introduced the reader to EMS of solids (see also the following paper by Vos 1998, present issue p. 609). It is the only means of obtaining momentum-density information for amorphous materials. Energy–momentum densities have also been observed for oriented crystals. This information is complementary to the dispersion curves that can be obtained by angle-resolved photoelectron spectroscopy with momenta uncertain up to the addition of an arbitrary reciprocal-lattice vector. Further understanding has been introduced by the observation of diffraction effects at certain critical angles of incidence. Much progress has been made in the preparation of 10 nm metal and semiconductor targets.

References

Adcock, W., Brunger, M. J., Clark, C. I., McCarthy, I. E., Michalewicz, M. T., von Niessen, W., Weigold, E., and Winkler, D. A. (1997). *J. Am. Chem. Soc.* **119**, 2896.

Bawagan, A. O., Brion, C. E., Davidson, E. R., and Feller, D. (1987). *Chem. Phys.* **113**, 19.

Camilloni, R., Giardini-Guidoni, A., Tiribelli, R., and Stefani, G. (1972). *Phys. Rev. Lett.* **29**, 618.

Canney, S. A., Vos, M., Kheifets, A. S., Clisby, N., McCarthy, I. E., and Weigold, E. (1997). *J. Phys.* C **9**, 1931.

Cook, J. P. D., McCarthy, I. E., Mitroy, J., and Weigold, E. (1986). *J. Phys.* B **17**, 2339.

Cook, J. P. D., McCarthy, I. E., Stelbovics, A. T., and Weigold, E. (1984). *J. Phys.* B **17**, 2339.

Dey, S., Dixon, A. J., McCarthy, I. E., and Weigold, E. (1976). *J. Elect. Spectrosc.* **9**, 397.

Dey, S., McCarthy, I. E., Teubner, P. J. O., and Weigold, E. (1975). *Phys. Rev. Lett.* **34**, 782.

Dixon, A. J., Dey, S., McCarthy, I. E., Weigold, E., and Williams, G. R. J. (1977). *Chem. Phys.* **21**, 81.

Duffy, P., Chong, D. P., Casida, M. E., and Salahub, D. R. (1994). *Phys. Rev.* A **50**, 4707.

Ehrhardt, H., Schulz, M., Tekaat, T., and Willmann, K. (1969). *Phys. Rev. Lett.* **22**, 89.
Froese-Fischer, C. (1972). *Atomic Data* **4**, 301.
Garron, J. P., Jacmart, J. C., Riou, M., Ruhla, C., Teillac, J., and Strauch, K. (1962). *Nucl. Phys.* **37**, 126.
Grant, I. P. (1970). *Adv. Phys.* **19**, 747.
Hayes, P. A., Williams, J. F., and Flexman, J. (1990). *J. Elect. Spectrosc.* **53**, 5.
Hood, S. T., Hamnett, A., and Brion, C. E. (1976). *Chem. Phys. Lett.* **39**, 252.
Hood, S. T., Weigold, E., McCarthy, I. E., and Teubner, P. J. O. (1973). *Nature (Phys. Sci.)* **245**, 65.
Lower, J., Bharathi, S. M., Chen, Y., Nygaard, K. J., and Weigold, E. (1991). *Microsc. Microanal. Microstruct.* **2**, 377.
McCarthy, I. E., and Mitroy, J. (1986). *Phys. Rev.* A **34**, 4426.
McCarthy, I. E., and Weigold, E. (1976). *Phys. Rep.* C **27**, 275.
McCarthy, I. E., and Weigold, E. (1988). *Rep. Prog. Phys.* **51**, 299.
McCarthy, I. E., Pascual, R., Storer, P. J., and Weigold, E. (1989). *Phys. Rev.* A **40**, 3041.
McLean, A. D., Weiss, A., and Yoshimine, M. (1960). *Rev. Mod. Phys.* **32**, 211.
Palke, W. E., and Lipscomb, W. N. (1966). *J. Am. Chem. Soc.* **88**, 2384.
Pitzer, R. M. (1967). *J. Chem. Phys.* **46**, 4871.
Ritter, A. L., Dennison, J. R., and Jones, R. (1984). *Phys. Rev. Lett.* **53**, 2054.
Snyder, L. C., and Basch, H. (1972). 'Molecular Wave Functions and Properties' (Wiley: New York).
Storer, P. J., Caprari, R. S., Clark, S. A. C., Vos, M., and Weigold, E. (1994). *Rev. Sci. Instrum.* **65**, 2214.
Vos, M. (1998). *Aust. J. Phys.* **51**, 609.
Vos, M., and Bottema, M. (1996). *Phys. Rev.* B **54**, 5964.
Weigold, E., Hood, S. T., and Teubner, P. J. O. (1973*a*). *Phys. Rev. Lett.* **30**, 475.
Weigold, E., Hood, S. T., McCarthy, I. E., and Teubner, P. J. O. (1973*b*). *Phys. Lett.* A **44**, 531.
Zheng, Y., McCarthy, I. E., Weigold, E., and Zhang, D. (1990). *Phys. Rev. Lett.* **64**, 1358.

Manuscript received 13 November 1997, accepted 10 February 1998